

## A Sensitivity Study of Radiative–Convective Equilibrium in the Tropics with a Convection-Resolving Model

KUAN-MAN XU AND DAVID A. RANDALL

*Department of Atmospheric Science, Colorado State University, Fort Collins, Colorado*

(Manuscript received 29 October 1997, in final form 24 December 1998)

### ABSTRACT

Statistical-equilibrium (SE) states of radiative–convective systems in tropical oceanic conditions are simulated with a cloud ensemble model (CEM) in this study. Typical large-scale conditions from the Marshall Islands and the eastern tropical Atlantic regions are used to drive the CEM.

The simulated SE precipitable water, column temperature, and relative humidity are only slightly higher than those of the observed mean states in both regions when time-invariant large-scale total advective cooling and moistening effects are imposed from observations. They are much higher than the observed if time-invariant observed large-scale ascent is imposed for the Marshall Islands region (i.e., ignoring horizontal advective effects). Compared with results from two similar studies, this SE state is somewhere between the cold/dry regime by Sui et al. and the warm/humid regime by Grabowski et al. Temporal variations of the imposed large-scale vertical motion that allows for subsidence make the SE state colder and drier. It remains about the same, however, if the magnitude of the imposed large-scale vertical motion is halved. The SE state is also colder and drier if solar radiation is absent. In general, all the SE states show that wet columns are thermally more stable (unstable) and dry columns are thermally more unstable (stable) in the lower (upper) troposphere.

Column budget analyses are performed to explore the differences among the simulations performed in this study and among the different studies.

### 1. Introduction

In radiative–convective systems, the thermodynamic state of the atmosphere ultimately comes into equilibrium with the convection. While such an equilibrium is inevitable in a time-averaged sense, it need not hold on a moment-by-moment basis. Thus, statistical equilibrium (SE) is a commonly used term to describe such not truly steady equilibrium states. A wide range of models have been used to investigate the SE states (Ramanathan and Oakley 1978; Randall et al. 1994), following the classic study of Manabe and Strickler (1964) and Manabe and Wetherald (1967), who used a one-dimensional (1D) model with parameterized convection. In such a model, certain assumptions on the SE state were built into the convective parameterization such as the existence of vertical eddy heat transport for preventing the lapse rate from increasing beyond a prescribed value. An assumption on the equilibrium humidity profile was also used, for example, a fixed relative humidity (Manabe and Wetherald 1967). The limiting lapse rate and the relative humidity profiles are typically taken from

the present climate. More comprehensive 1D models also prescribe fixed cloud amounts and optical properties for radiative calculation (e.g., Somerville and Remer 1984) or include an explicit hydrological cycle (Rennó et al. 1994).

Recently, more complicated, convection-resolving models have been used to examine radiative–convective systems and their statistical equilibria under different large-scale conditions (Nakajima and Matsuno 1988; Held et al. 1993; Islam et al. 1993; Sui et al. 1994; Grabowski et al. 1996; Robe and Emanuel 1996; Tompkins and Craig 1998). Such models replace those assumptions used in 1D models with explicit simulations of cloud formation and dissipation, eddy heat and moisture transports, as well as cloud–radiation interactions in two-dimensional (2D) or three-dimensional (3D) settings. These models feature explicit cloud-scale dynamics, bulk cloud microphysics, high-order turbulence closure, and interactive radiative transfer. All these processes are physically linked within the models. They therefore represent a valuable new generation of tools with which to study radiative–convective systems and their statistical equilibria.

One type of study is to examine the radiative–convective equilibrium without any large-scale forcing (Nakajima and Matsuno 1988; Islam et al. 1993; Held et al. 1993; Robe and Emanuel 1996; Tompkins and Craig

---

*Corresponding author address:* Dr. Kuan-Man Xu, Department of Atmospheric Science, Colorado State University, Fort Collins, CO 80523.  
E-mail: kmxu@atmos.colostate.edu

1998). Radiative heating/cooling rates were prescribed in Nakajima and Matsuno (1988), Islam et al. (1993), and Robe and Emanuel (1996). Held et al. (1993) and Tompkins and Craig (1998) studied a purely radiative–convective equilibrium with interactive radiation. In such systems, cumulus convection is driven by radiative cooling of the atmosphere and by sensible and latent heat fluxes from the underlying ocean. Held et al. (1993) used a 2D model with a horizontal grid of 5 km and a domain size of 640 km, while Tompkins and Craig (1998) used a 3D model with a horizontal grid of  $2 \times 2 \text{ km}^2$  and a domain size of  $100 \times 100 \text{ km}^2$ . Their simulations achieved statistical equilibria, but with strong low-frequency oscillations in the mean winds (Held et al. 1993) and in the thermodynamic fields (Tompkins and Craig 1998).

Another type of study is to simulate the radiative–convective equilibrium response to an imposed profile of rising motion or observed large-scale advective forcings (Sui et al. 1994; Grabowski et al. 1996). Both Sui et al. (1994; hereafter S94) and Grabowski et al. (1996; G96) used the observed large-scale vertical velocity profile over the Marshall Islands region (a pentagonal region centered at  $165^\circ\text{E}$  and  $9^\circ\text{N}$ ) with 2D cloud ensemble models (CEMs). The imposed large-scale advective cooling and moistening effects are dependent upon the simulated, domain-averaged temperature and moisture profiles. The simulated SE states in S94 and G96 are dramatically different in spite of similar models and experiment designs (e.g., a fixed sea surface temperature of  $28^\circ\text{C}$ ): (i) the SE precipitable water is  $51 \text{ kg m}^{-2}$  in S94 and  $70 \text{ kg m}^{-2}$  in G96, compared with an observed mean value of  $54 \text{ kg m}^{-2}$ , which was a 3-month average in the Marshall Islands region (Yanai et al. 1976); (ii) the SE column temperature is 258 K in S94 and 263 K in G96, compared with an observed mean value of 260 K; and (iii) the simulated vertical profiles of relative humidity are not similar to each other or to observations. G96 characterized its SE state as a warm and humid regime, as opposed to the cold and dry regime of S94.

One must wonder and perhaps be puzzled by why these two models produced such dramatically different regimes. In other words, do they merely represent intermodel differences in simulating radiative–convective equilibrium response to an imposed large-scale forcing? Recently, W.-K. Tao et al. (1999, personal communication) attributed the two different regimes to the difference in the surface fluxes, as resulted from the large deviation of the surface wind speed of the SE state from the initial state in S94. If the intermodel differences are indeed the cause, a simpler design of numerical simulations should be adopted in order to compare simulated SE states with the observed mean states. For a meaningful comparison with observations, one must prescribe both the vertical and horizontal advective cooling and moistening effects in the model. By prescribing the total advective effects, it eliminates the feedbacks of the simulated, domain-averaged temperature and moisture

on the vertical advection. Thus, the first objective of this study is *to examine how well a CEM performs against the observations of a particular, tropical oceanic region in simulating the SE states, driven by the observed large-scale forcings over the same region.*

The University of California, Los Angeles–Colorado State University (UCLA–CSU) CEM (Krueger 1988; Xu and Krueger 1991) is used in this study. This model is similar to those used by S94 and G96 except for a more sophisticated third-order turbulence closure. As in S94 and G96, it is a two-dimensional model, based on anelastic dynamics. It includes a three-phase bulk cloud microphysics parameterization (Lin et al. 1983; Krueger et al. 1995) and an interactive radiative transfer scheme (Harshvardhan et al. 1987; Xu and Randall 1995a). It differs from that in S94 in that the Coriolis force is included, which prevents the initial wind profile from changing drastically in long-term integrations (see Fig. 1) but allows for the temporal variation of the domain-averaged horizontal wind at the inertial timescale. Another difference lies at the treatment of the gustiness factors in the bulk formula for calculating the surface sensible and latent heat fluxes. A  $3 \text{ m s}^{-1}$  gustiness speed is used in this study, but none in S94.

The second objective of this study is *to compare the simulated, radiative–convective equilibrium response to an imposed large-scale vertical ascent by the UCLA–CSU CEM with S94 and G96.* A key question to be addressed is what experiment designs in either S94 or G96 are the probable causes for the two dramatically different regimes. As will be discussed later, there are some other possible causes, in addition to that given by Tao et al. (1999). Detailed budget analyses will also be performed to investigate the differences among the three modeling studies.

The last objective of this study is *to examine the sensitivity of the SE states to the imposed large-scale conditions* such as the magnitude and the temporal variation of the large-scale vertical motion, the absence of solar radiation, and the geostrophic wind profiles. The results can be used to discuss the limited relevance of the simulated SE states to the tropical dynamics.

## 2. Numerical experiments

A series of explicit cumulus ensemble simulations is performed to examine the radiative–convective equilibrium in the tropical atmosphere. Typical large-scale conditions over tropical oceanic locations such as the Marshall Islands (western Pacific) and the eastern Atlantic regions are used to drive the CEM for the simulations described below. Two control simulations are performed to address the first objective outlined in section 1. Also performed are several sensitivity simulations (Table 1). A general rule for naming these simulations is as follows. The upper case denotes the type of the forcings: M for the Marshall Islands region, G for the GATE region, and W for being forced by vertical motion only.

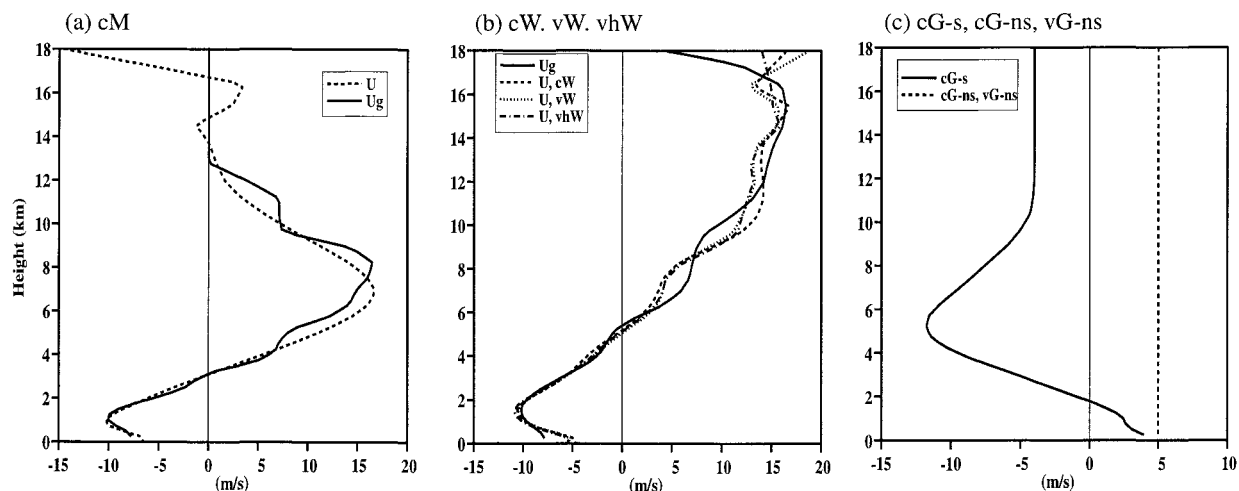


FIG. 1. Vertical profiles of the  $x$ -component geostrophic winds used in simulations (a) cM; (b) cW, vW, and vhW; and (c) cG-s, cG-ns, and vG-ns. (a), (b) the  $x$ -component winds averaged over the last 10 days of those simulations are also shown.

The lower case(s) ahead of the upper case denotes the temporal variation of the forcing: c (constant), v (varying in time), and h (half of the magnitude). The lower case(s) after a hyphen indicates the type of geostrophic wind: s for sheared, and ns for nonsheared. A sheared profile is used if a hyphen does not appear in the name.

#### a. Control simulations

In the simulations performed by S94 and G96, the large-scale advective cooling and moistening are imposed via a given profile of large-scale vertical velocity. Therefore, the large-scale, horizontal advection of temperature and moisture is totally ignored for a given large-scale condition. In some regions of the Tropics, the large-scale, horizontal advective effects are not always negligible, especially the horizontal moisture advection. Therefore, in the control simulations performed, the vertical profiles of the mean, total advective cooling and moistening effects (Figs. 2a,b) are imposed on the model grid points, uniformly in  $x$ . These advective effects are assumed to be time invariant.

Simulation cM represents the control simulation for the Marshall Islands region, using the total advective

cooling and moistening profiles (Fig. 2a) obtained by Yanai et al. (1973). A sheared geostrophic wind profile (Fig. 1a) is used to prescribe the  $y$ -component pressure gradient in the model. This profile is similar (should be identical, but it is not, due to an interpolation error) to the initial profile used in S94 and G96. This should not impact the simulated SE state because the surface wind speeds are identical. Both diurnally varying solar and infrared radiation are included in the simulation. The SST is fixed at 28°C, as in S94 and G96. The Coriolis parameter at 8.5°N is used. The simulation was run for 29 days of physical time.

Simulations cG-s and cG-ns represent the control simulations for the eastern Atlantic region using the Global Atmospheric Research Program's Atlantic Tropical Experiment (GATE) Phase III mean profiles (Fig. 2b). The magnitudes of the advective cooling and moistening rates are twice the observed, but this does not greatly affect the simulated SE states, as evidenced by the comparison between vW and vhW (see section 4c). Both simulations include solar and infrared radiation. The only difference between cG-s and cG-ns is whether or not a sheared geostrophic wind profile is used to prescribe the  $y$ -component pressure gradient in the model;

TABLE 1. A list of numerical simulations performed in this study.

Expt	Time variation of forcing	Type of large-scale forcing	Radiation	SST (C)	Geostrophic wind	Averaging period for SE state
cM	Steady	Total advective effects	SW + LW	28.0	Sheared	1–29 days
cG-s	Steady	Total advective effects	SW + LW	26.7	Sheared	1–21 days
cG-ns	Steady	Total advective effects	SW + LW	26.7	No shear	1–16 days
cW	Steady	Vertical velocity ( $w$ )	SW + LW	28.0	Sheared	28–38 days
vW	Varying	Vertical velocity ( $w$ )	SW + LW	28.0	Sheared	28–38 days
vhW	Varying	Vertical velocity (1/2 $w$ )	SW + LW	28.0	Sheared	1–29 days
vG-ns	Varying	Total advective effects	LW only	26.7	No shear	10–19 days

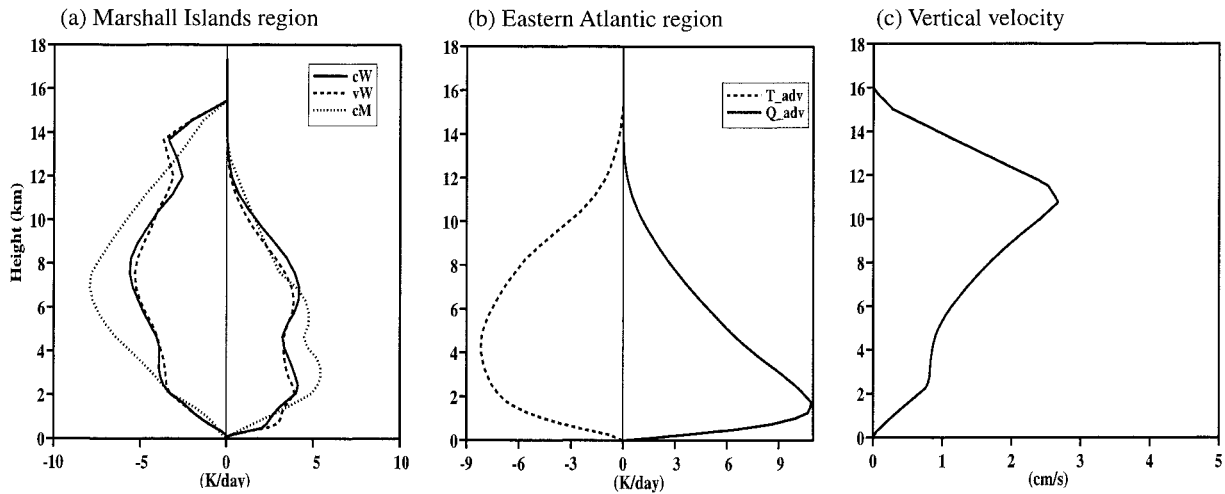


FIG. 2. Vertical profiles of the imposed (a) large-scale advective cooling and moistening in cM and the vertical advective cooling and moistening for the SE states of cW and vW, (b) large-scale advective cooling and moistening for simulations in the eastern Atlantic regions (cG-s, cG-ns, vG-ns), and (c) imposed large-scale vertical velocity in cW, vW, and vhW.

that is, cG-s uses a sheared profile (a typical low-level easterly jet) while cG-ns uses a nonsheared profile with an identical surface wind speed as in the sheared profile (Fig. 1c). In fact, cG-ns identical to I05 in Xu and Randall (1995b), which was used to study the mechanisms of cloud diurnal variations. The length of the integration is 16 days for cG-ns and 21 days for cG-s. The SST is fixed at 26.7°C in both runs, typical of the GATE region (Krishnamurti et al. 1976). The Coriolis parameter at 9°N is used in these two simulations.

### b. Sensitivity simulations

The first three simulations described below are performed with a large-scale vertical motion profile based on observations from the Marshall Islands region, two of which address the second objective outlined in section 1. The design of cW closely follows that by S94 and G96 [see W.-K. Tao et al. (1999, personal communication) for the differences between S94 and G96]. Unlike cM, the large-scale advective effects are imposed on the model grid points via a vertical velocity profile (Fig. 2c). As in G96W.-K., the diurnally varying solar insolation is used. S94 used a daily-mean solar insolation in their simulation. The geostrophic (and initial) wind profile in cW (Fig. 1b) is identical to that in S94 and G96, and so is the SST.

A steady uplifting profile used in cW does not allow any suppressed condition over a significantly long period. As shown later, this can influence the simulated SE state under a given large-scale condition. Thus, simulation vW is performed with a time-varying vertical motion profile; that is, vW is identical to cW except that the prescribed large-scale, vertical velocity profile is assumed to vary with time according to

$$f(t) = 1 + 2 \cos(2\pi t/T), \quad (1)$$

where  $T$  is the period of the time variation, which is chosen to be 54 h. It is approximately the period of the observed easterly waves in the Marshall Islands region (Yanai et al. 1976).

The rest of the simulations are performed to address the third objective outlined in section 1. Simulation vhW is identical to vW except for halving the magnitude of the imposed large-scale vertical velocity. This simulation is intended to examine whether or not the SE state is dependent upon the magnitude of the imposed large-scale advective effects.

Simulation vG-ns is performed for the eastern Atlantic region to examine the impact of solar radiation on the SE state. Thus, vG-ns is performed with longwave radiation but without solar radiation. Its designs are similar to cG-ns described above except for the time variation of the imposed large-scale advective effects. This simulation is identical to Ctrl in Xu and Randall (1998). Further details can be found in that paper.

The length of the integration is 38 days for cW and vW but 29 days for vhW and cM. It is shorter in vhW and cM because the SE states are more quickly reached. Nevertheless, these integration lengths are longer than that in G96 (24 days) but shorter than that in S94 (52 days). In all simulations, the horizontal domain size is 512 km, with a horizontal grid size of 2 km and a time step of 10 s. There are only 33 layers in the vertical. The vertical grid spacing ranges from 100 m near the ocean to 1000 m near the model top (at 19 km).

## 3. Results from the control simulations

The temporal evolution of domain-averaged precipitable water for simulations cM, cG-s, and cG-ns is shown in Fig. 3. A 3-h average is used to give a smooth time-series plot. The most interesting feature shown in

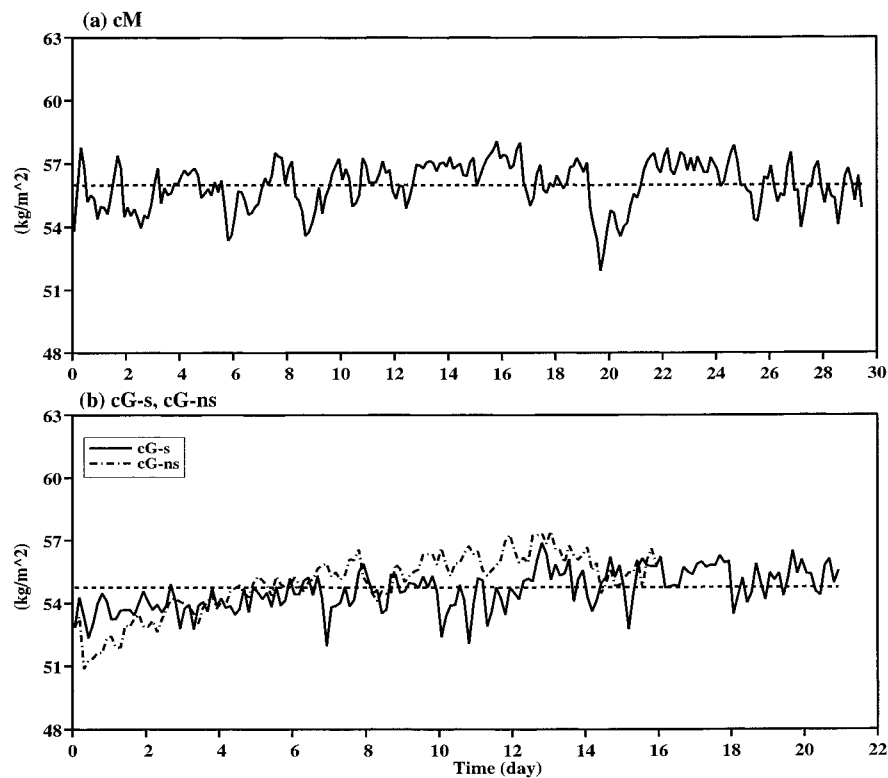


FIG. 3. Time sequence of the domain-averaged precipitable water for (a) simulation cM, and (b) simulations cG-s and cG-ns. The horizontal dashed lines indicate the SE states.

Fig. 3 is that the simulated precipitable water in these three simulations does not deviate much from the initial value, which is the observed mean state in both the Marshall Islands and the eastern Atlantic regions, in spite of the fact that there are some high-frequency fluctuations. As explained by Xu et al. (1992), these fluctuations represent the stochastic aspects of simulated deep convection, which can be related to the existence of organized mesoscale convective systems and the diurnal cycle of solar radiation. A larger horizontal domain would reduce the magnitudes of the high-frequency fluctuations (Xu et al. 1992), and so would a 3D model.

The 29-day mean<sup>1</sup> precipitable water for cM is  $56 \text{ kg m}^{-2}$ , with a standard deviation of only  $1.1 \text{ kg m}^{-2}$ . This is only  $2 \text{ kg m}^{-2}$  higher than that of the observed mean state (a 3-month average) in the Marshall Islands region (Yanai et al. 1976). The column temperature in cM (not shown) is rather close to the initial value, with a 29-day mean of 259.6 K. Therefore, cM produces the precipitable water and column temperature rather close to those observed in the Marshall Islands region. This is

<sup>1</sup> The mean over the entire integration period is chosen to represent the SE state of the control simulations, due to small deviations from the initial condition.

an expected result (due to the imposed total advective forcings) if the model behaves similarly as in the real atmosphere. However, the idealized nature of the temporal variation of the imposed forcings and the periodic lateral boundary condition could impact the similarities between simulations and observations.

The SE precipitable water for the eastern Atlantic region, averaged over the full length of simulation, is about  $55 \text{ kg m}^{-2}$  in both simulations whether the geostrophic wind has its vertical shear or not (Fig. 3b). Note that the surface wind speeds (Fig. 1c) are identical in these simulations so that the surface fluxes do not differ much. The SE precipitable water is also  $2 \text{ kg m}^{-2}$  higher than the initial state, which is from the GATE Phase III mean profile (a 20-day average in September 1974). The SE column temperatures (not shown) only differ by 0.7 K: 260.4 K for cG-ns and 259.7 for cG-s. They are also close to that of the observed mean state (260 K).

A comparison of the vertical profiles of simulated and observed relative humidities (RHs) is also made (Fig. 4). The observed RH profiles were kindly provided by C.-H. Sui (see Fig. 9 in S94). A noticeable feature in Fig. 4a is that the observed minimum RH at 7 km and the maximum RH at 14 km are simulated by cM in spite of overestimates of 10%–15% below 12 km. Note that measurements of RHs above 250 mb ( $\sim 10.5 \text{ km}$ ) are

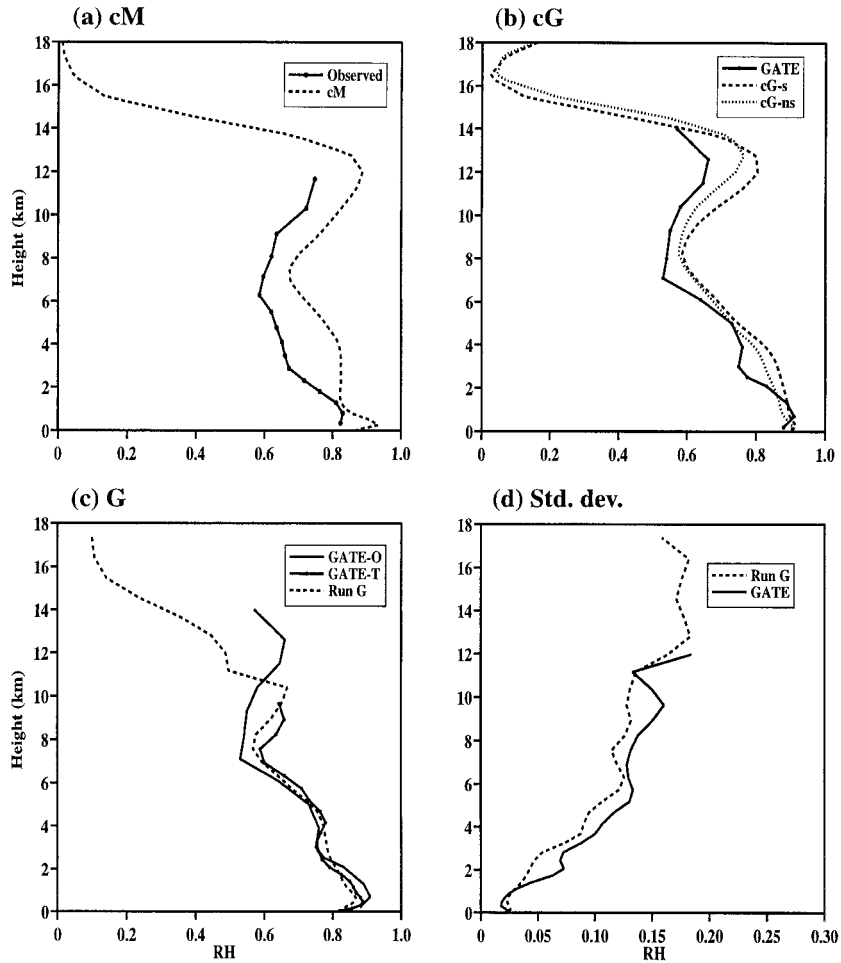


FIG. 4. Vertical profiles of the SE relative humidity for (a) simulation cM, and (b) simulations cG-s and cG-ns. The observed mean RHs for (a) the Marshall Islands region and (b) the eastern Atlantic (GATE) region; (c), (d) the mean and standard deviations of RH for run G, performed by Xu and Randall (1996). (c) Analyses by Esbensen and Ooyama (GATE-O) and Thompson et al. (GATE-T) are shown.

not reliable. That is, the comparison between observation and simulation is not meaningful above 10.5 km. The good agreement of the RH profiles between cM and observation suggests the importance of including the horizontal advective effects, which was totally neglected in either S94 or G96. The overestimates of 10%–15% below 12 km, which are comparable to the standard deviations of observed RHs (5%–15%) in the Marshall Islands region, could be caused by the idealization of the temporal evolutions of the observed large-scale forcings, that is, time invariant in cM, and the periodic lateral boundary condition. The latter forces the condensate to remain inside the horizontal domain, which impacts the moisture and cloud–radiation interactions.

For the eastern Atlantic region, the simulated RH profiles are extremely similar to that observed during GATE Phase III except for slight overestimates between 1 and 14 km (Fig. 4b). The overestimates shown in Figs. 4a and 4b are only slightly greater than the uncertainty of

measurements/analyses (Fig. 4c). The differences of the mean RHs as analyzed by Esbensen and Ooyama (1983) and Thompson et al. (1979) are as large as 10% above 8 km. As shown in section 4, they are smaller than the differences among the different studies for the Marshall Islands region.

Since both cG-s and cG-ns are idealized experiments, one may question whether the CEM simulates the observed RH profiles well with observed large-scale conditions. The mean and standard deviations of RHs from simulation G, as performed by Xu and Randall (1996) with observed time-varying large-scale forcings and wind profiles during the entire GATE Phase III, are shown in Figs. 4c and 4d. The agreement between observation and simulation is remarkably good, as far as the mean and standard deviations of RHs are concerned. This gives us additional confidence regarding the performance of the UCLA–CSU CEM.

Comparisons of the SE temperature and water vapor

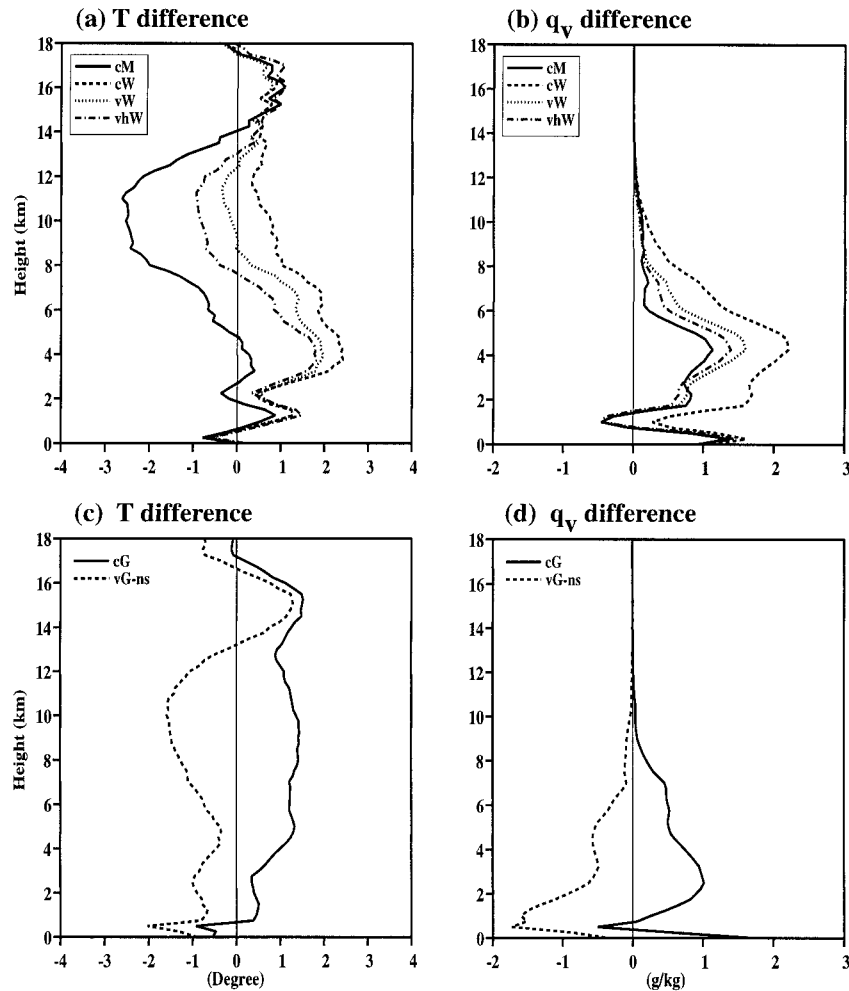


FIG. 5. Same as Fig. 4 except for the temperature and water vapor mixing ratio differences from the observations for simulations cM, cW, vW, vhW, cG, and vG-ns.

mixing ratio profiles are also made against observations from the Marshall Islands (Figs. 5a and 5b) and from the eastern Atlantic regions (Figs. 5c,d). In the plots, cG denotes an average of cG-s and cG-ns. It appears that the differences from the respective observations are small (1 K or 1 g kg<sup>-1</sup>, typical magnitudes of the observed standard deviations in the Tropics), except for the differences of -2.5 K in the upper troposphere of

cM. These results suggest that the UCLA-CSU CEM reproduces the observed mean temperature and moisture profiles of two tropical regions reasonably well.

The reasons for the overestimates of RHs shown in Fig. 4 are not identical between the two regions, based on the results from Fig. 5. The large underestimate of temperature in the middle and upper troposphere and the overestimate of moisture in the lower troposphere are responsible for the overestimate of RHs in cM. On the other hand, the slight overestimates of both temperature and moisture account for the smaller overestimates of RHs in cG.

The convective and stratiform precipitation are also compared among the simulations (Table 2). The method for partitioning convective and stratiform areas was proposed by Xu (1995), based on the strength of updrafts and downdrafts. The percentage of convective (stratiform) precipitation is 63% (38%), 54% (46%), and 44% (56%) for cG-ns, cG-s, and cM, respectively. That is, the stratiform precipitation is more abundant when the

TABLE 2. Percentages of convective ( $P_c$ ) and stratiform ( $P_s$ ) precipitation and convective ( $A_c$ ) and stratiform ( $A_s$ ) areas for each simulation.

Simulation	$P_c$ (%)	$P_s$ (%)	$A_c$ (%)	$A_s$ (%)
cM	43.9	56.1	7.4	31.0
cG-ns	63.2	36.8	8.1	24.2
cG-s	53.8	46.2	8.5	28.5
cW	41.7	58.3	7.0	36.7
vW	50.8	49.2	5.4	23.2
vhW	48.8	51.2	4.9	20.0
S94	68.0	32.0	n/a	n/a

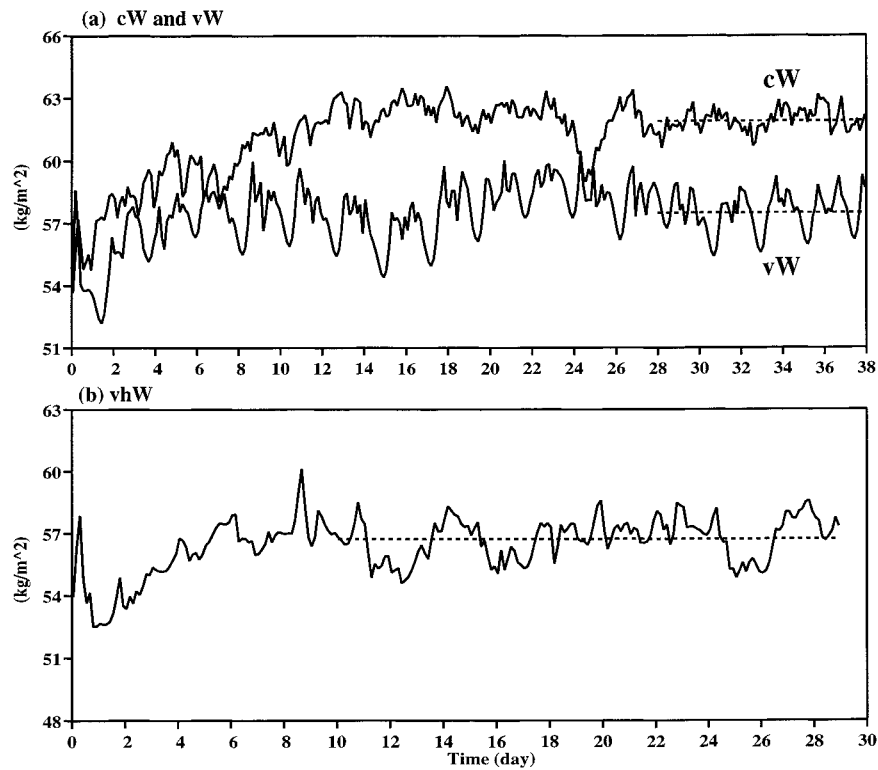


FIG. 6. Time sequence of the domain-averaged precipitable water for (a) simulations cW and vW, and (b) simulation vhW. The horizontal dashed lines indicate the averaged value that represents the SE state.

geostrophic winds have vertical shear, due to the presence of stronger mesoscale circulations. The convective areas (between 7.4% and 8.5%) do not differ much among the simulations. The stratiform areas are, however, proportional to the stratiform precipitation amount, with the smallest area in the nonsheared simulation.

In summary, the UCLA–CSU CEM has performed reasonably well against the observed mean states over two tropical regions in simulating the SE states. Such a good agreement between simulations and observations is prerequisite to perform sensitivity studies of the SE states to the imposed large-scale conditions.

#### 4. Results from the sensitivity simulations

##### a. Comparison among the three modeling studies

Simulation cW is used to compare the simulated, radiative–convective response to an imposed large-scale vertical ascent by the UCLA–CSU CEM with S94 and G96. The simulated precipitable water in cW reaches over  $60 \text{ kg m}^{-2}$  after the initial adjustment (Fig. 6a). The SE value (from 28 to 38 days) is  $61.9 \text{ kg m}^{-2}$ , with a standard deviation of only  $0.5 \text{ kg m}^{-2}$ . Note that averaging over a longer period starting from day 10 of cW and vW would not change the SE states at all. The SE precipitable water is about  $8 \text{ kg m}^{-2}$  ( $6 \text{ kg m}^{-2}$ ) higher than the observed mean (simulation cM) for the

Marshall Islands region. It is, however, about  $8 \text{ kg m}^{-2}$  lower than that simulated by G96.

S94 obtained an SE precipitable water of  $51.3 \text{ kg m}^{-2}$  in a similar simulation, which is lower than the observed mean state over the Marshall Islands region. An explanation regarding the low value in S94 was offered by W.-K. Tao et al. (1999, personal communication). Similar differences among the three studies also appear in the the density-weighted column temperature (not shown). The SE column temperature is  $261.2 \text{ K}$  for cW, which is about  $1 \text{ K}$  higher than the initial value. It is lower than that ( $263 \text{ K}$ ) simulated by G96, but much higher than that ( $257.6 \text{ K}$ ) simulated by S94. Thus, the differences among the three modeling studies are significant. More differences are shown below.

A comparison of simulated RHs among the SE states of cW, S94, and G96 (against the observation) is revealing (Fig. 7a). Below  $5.5 \text{ km}$ , all simulated RHs are higher than that of the observed mean state. The RHs in cW are close to those in S94 below  $4.5 \text{ km}$  except for the slightly more humid boundary layer. The RHs in G96 are close to  $90\%$  between  $0$  and  $7 \text{ km}$ ; they are much higher than in either S94 or cW. Another feature in Fig. 7a is that the simulated RHs above  $5 \text{ km}$  deviate from each other very significantly. None of them captures the observed minimum at  $7 \text{ km}$ . For example, the simulated upper troposphere in S94 is much drier than

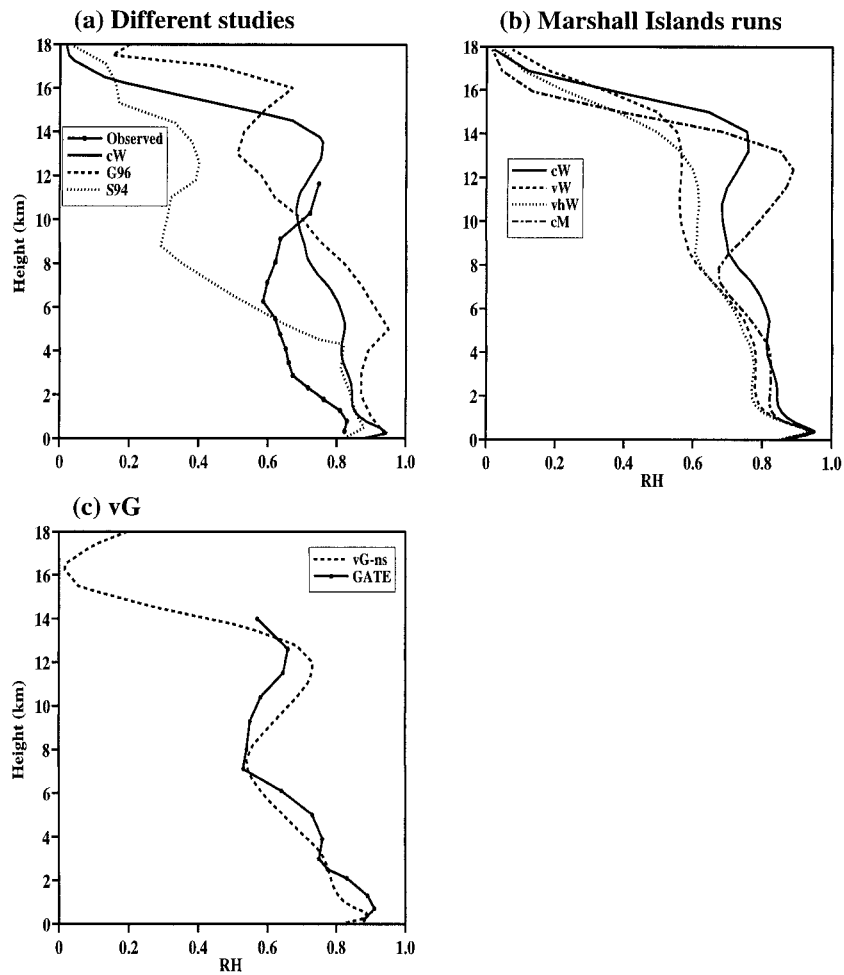


FIG. 7. Vertical profiles of the SE relative humidity for (a) different studies, (b) Marshall Islands simulations, and (c) vG-ns. Observed mean RHs for (a) the Marshall Islands region and (c) the eastern Atlantic (GATE) region are also shown.

the observed. The entire troposphere simulated by G96 is more humid than in cW except for between 10 and 15 km, where the observed RHs are not reliable. In a word, the intermodel differences are much larger than the observed standard deviations (5%–15%) throughout the entire troposphere. These intermodel RH differences indicate that the simulated interactions between clouds and radiation are not similar.

The differences in the mixing ratio of the various water species are also significant among cW, S94, and G96 (Fig. 8), especially in the upper troposphere. This is expected in view of the large RH differences discussed above. For example, the sum of cloud ice, snow, and graupel in G96 is five times greater than in cW and S94 (Fig. 8b). The mixing ratios of cloud ice and snow in S94 are much smaller than in cW but that of graupel is much larger (Fig. 8d), which is a consequence of the drier upper troposphere in S94. The sums of cloud water and rainwater mixing ratios also show appreciable differences among the three simulations (Fig. 8a), and so

do the cloud water and rainwater mixing ratios between cW and S94 (Fig. 8c). In addition, S94 produces far less stratiform precipitation than in cW (32% vs 58%; Table 2), due to the less sheared wind profile of the SE state in S94.

The differences among the three studies can be explained by the column budgets. The column moist static energy  $\langle \bar{h} \rangle$ , dry static energy  $\langle \bar{s} \rangle$ , and moisture  $\langle \bar{q} \rangle$  budgets are expressed as follows:

$$\left\langle \frac{\partial \bar{h}}{\partial t} \right\rangle = \left\langle \left( \frac{\partial \bar{h}}{\partial t} \right)_{\text{is}} \right\rangle + \langle Q_R \rangle + LE + H_s, \quad (2)$$

$$\left\langle \frac{\partial \bar{s}}{\partial t} \right\rangle = \left\langle \left( \frac{\partial \bar{s}}{\partial t} \right)_{\text{is}} \right\rangle + \langle Q_R \rangle + H_s + LP, \quad (3)$$

$$L \left\langle \frac{\partial \bar{q}}{\partial t} \right\rangle = L \left\langle \left( \frac{\partial \bar{q}}{\partial t} \right)_{\text{is}} \right\rangle - LP + LE, \quad (4)$$

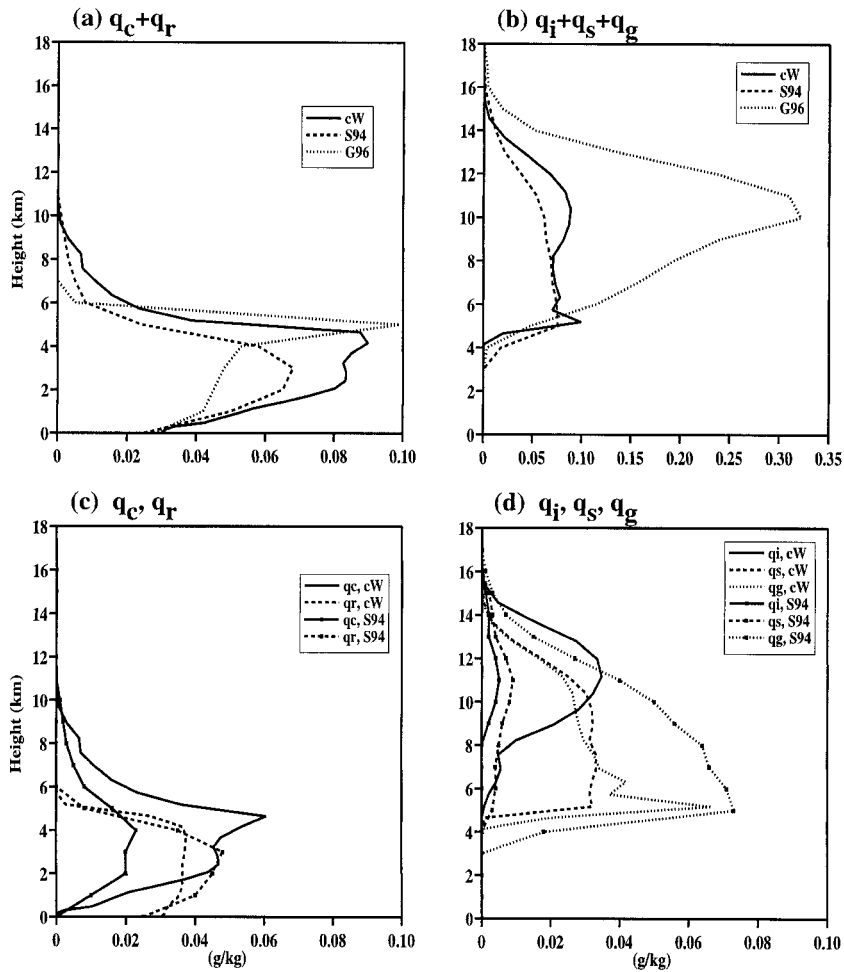


FIG. 8. Vertical profiles of the mixing ratios of water species for simulation cW of this study, S94 and G96: cloud water ( $q_c$ ), cloud ice ( $q_i$ ), rainwater ( $q_r$ ), snow ( $q_s$ ), and graupel ( $q_g$ ).

where the angle brackets denote the vertical mass integrals from the bottom to the top of the model atmosphere,  $Q_R$  is the radiative heating rate,  $E$  is the surface evaporation rate,  $P$  is the surface precipitation rate,  $H_s$  is the surface sensible heat flux, and  $L$  is the latent heat of vaporization. The subscript “ls” denotes the large-scale advective effects. Tables 3, 4, and 5 show the individual budget terms for the SE states.

The greatest differences between cW and S94 appear in  $LP$  and the large-scale advective effects (Tables 3–5). This suggests that the feedback of simulated temperature and moisture on the vertical advective effects is rather different between the two simulations. The surface precipitation in S94 is larger than in cW by 27%. The difference of  $14 \text{ W m}^{-2}$  in  $\langle Q_R \rangle$  is caused by a small amount of upper-tropospheric clouds simulated by S94 due to the extremely dry upper troposphere (Fig. 7a). This difference may also be attributed to the difference in the cloud optical thickness. In spite of the drier and cooler boundary layer (than in cW), the simulated  $H_s$  and  $LE$  in S94 are very close to those simulated by cW.

This is due to the inability of its model to maintain the initial wind profile in S94, which greatly reduces the surface wind speed (W.-K. Tao et al. 1999, personal communication). The initial wind profiles are, however, maintained in this study (see Fig. 1). Thus, the explanation given by W.-K. Tao et al. (1999, personal communication), based upon the surface fluxes, may not be the only one for the cold/dry SE state of S94 because

TABLE 3. Individual terms of the column moist static energy budget for SE states. Unit is  $\text{W m}^{-2}$ . In G96,  $\langle \delta h / \delta t \rangle_{ls}$  inside parentheses is obtained from the budget requirements.

Simulation	$LE$	$H_s$	$\langle Q_R \rangle$	$\langle \delta h / \delta t \rangle_{ls}$
cW	118	14	-109	-23
vW	133	14	-117	-30
cM	145	16	-104	-57
S94	120	18	-95	-43
G96	94	10	-40	+81 (-64*)
cG	96	13	-109	0
vG-ns	138	33	-195	+24

TABLE 4. Same as Table 3 except for the column dry static energy budget. In  $\langle Q_R \rangle$  column, the solar radiative flux is included in parentheses.

Simulation	$LP$	$H_s$	$\langle Q_R \rangle$	$\langle \delta s / \delta t \rangle_s$
cW	398	14	-109 (88)	-303
vW	402	14	-117 (87)	-299
cM	456	16	-104 (89)	-368
S94	507	18	-95 (92)	-430
G96	486	10	-40 (nla)	-405 (-456*)
cG	653	13	-109 (89)	-557
vG-ns	395	33	-195 (0)	-233

the feedback of soundings on the large-scale advective effects is much stronger in S94 than in cW.

On the other hand, the comparison with G96 is difficult because there is an imbalance of  $70 \text{ W m}^{-2}$  in the moisture budget and  $51 \text{ W m}^{-2}$  in the dry static energy budget of G96, based on the information extracted from Figs. 14 and 15 of G96. For reference, the advective effects are also obtained from the budget requirements, shown with an asterisk in Tables 3–5. Nevertheless, the most significant difference among G96, S94, and cW appears in the radiative flux ( $-40 \text{ W m}^{-2}$ ). Such a small cooling is due to strong solar heating in the upper troposphere (Fig. 6 in G96). Based on the budget imbalances and the small  $\langle Q_R \rangle$ , the SE state obtained by G96 should be treated with caution. The imbalances could be also due to (i) infrequent sampling of surface precipitation data and (ii) nonconservative numerics in the model. G96 noticed these imbalances as well before but decided not to comment on the paper (W. Grabowski 1997, personal communication). On the other hand, the smaller  $H_s$  and  $LE$  are consistent with the warmer and more moist boundary layer simulated by G96 since the initial surface wind speed is also maintained during the simulation.

#### b. Sensitivity to transient large-scale forcings

A possible reason for the high precipitable water in simulation cW is that the steady uplifting does not allow any suppressed condition to occur over a significantly long period so that moisture and hydrometeor are not depleted as much as in the real atmosphere. In reality, suppressed conditions occur as frequently as active convection periods. The simulated precipitable water in vW never exceeds  $60 \text{ kg m}^{-2}$  (Fig. 6a). The SE value (from 28 to 38 days) is  $57.5 \text{ kg m}^{-2}$ , with a standard deviation

TABLE 5. Same as Table 3 except for the column moisture budget.

Simulation	$LP$	$LE$	$L\langle \delta q / \delta t \rangle_s$
cW	398	118	280
vW	402	133	269
cM	456	145	311
S94	507	120	387
G96	486	94	462 (392*)
cG	653	96	557
vG-ns	395	138	257

of  $0.9 \text{ kg m}^{-2}$ . This is much closer to the observed mean precipitable water. The SE column temperature (not shown) in vW is only lower than in cW by  $0.2 \text{ K}$ .

Evidence of accumulation of moisture and hydrometeor can be clearly seen from Figs. 5b and 9 by comparing their vertical profiles between cW and vW. That is, the water vapor mixing ratio in cW is about  $0.5 \text{ g kg}^{-1}$  higher than in vW in the lower and middle troposphere. The mixing ratios of cloud water, cloud ice, and snow in cW are also higher than in vW by 10%–30% at selected levels. Through the interaction with radiation, the temperature in vW is also slightly lower than in cW:  $0.5$ – $1.0 \text{ K}$  in the middle and upper troposphere (Fig. 5a). This is a consequence of the longwave cooling during extended suppressed conditions (Table 4). Thus, the RH shows the largest differences between vW and cW in the middle and upper troposphere (Fig. 7b).

In the column budgets, the most significant differences between cW and vW are in the surface latent heat flux and the radiative flux. Simulation vW shows a larger surface latent heat flux ( $15 \text{ W m}^{-2}$ ), which is almost compensated by the reduced large-scale moistening (Table 5). The larger surface latent heat flux implies that the boundary layer is drier, which reduces the amount of precipitable water. The radiative cooling in vW is greater than in cW by  $8 \text{ W m}^{-2}$ , due to the presence of extended suppressed conditions and less vapor.

An implication from the comparison between vW and cW is that an accumulation of condensate and its interaction with radiation can significantly alter the simulated SE state, especially in the water cycle.

#### c. Sensitivity to magnitudes of large-scale forcings

As in vW, the simulated precipitable water in vhW does not differ much from the initial value (Fig. 6b). The differences are that the high-frequency fluctuations in vhW are largely dominated by the diurnal variations, whereas those in vW are dominated by large amplitudes of variations associated with the imposed large-scale forcing (Fig. 6a). The 29-day mean precipitable water is  $56.5 \text{ kg m}^{-2}$ , with a standard deviation of  $1.3 \text{ kg m}^{-2}$ . This is  $1.0 \text{ kg m}^{-2}$  lower than in vW. The mean column temperature is  $260.7 \text{ K}$ , compared with  $260.9 \text{ K}$  in vW. The small differences between vhW and vW also appear

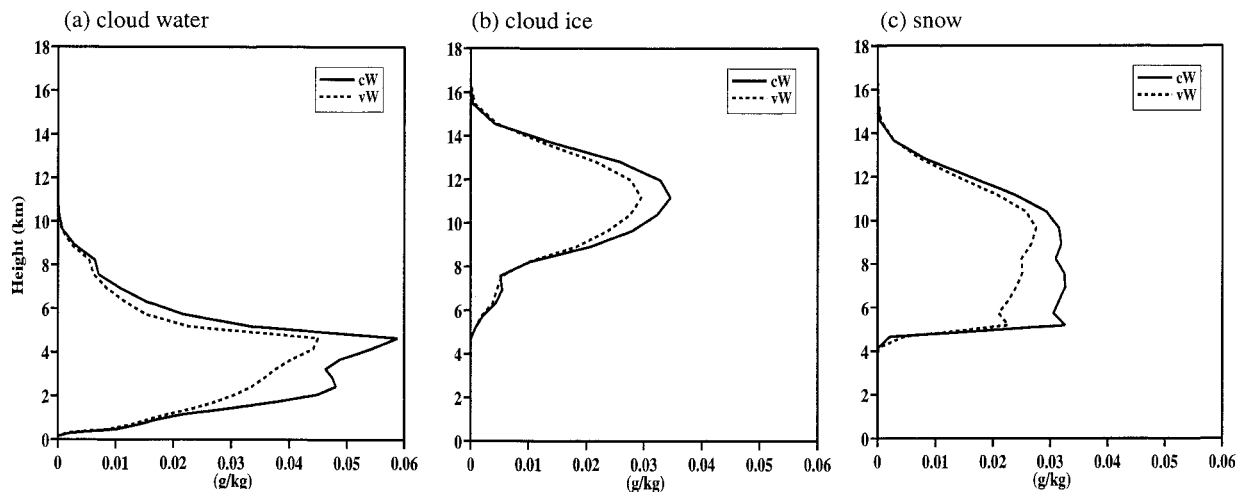


FIG. 9. Vertical profiles of the mixing ratios of (a) cloud water, (b) cloud ice, and (c) snow averaged over the entire domain in space and 36 days in time for cW and vW.

in the vertical profiles of temperature (Fig. 5a), water vapor mixing ratio (Fig. 5b), and RH (Fig. 7b). Therefore, the SE state does not strongly depend upon the magnitude of the large-scale vertical motion. This may not be true if the amplitude of the large-scale uplifting is reduced to zero.

#### d. Sensitivity to radiation

The SE state for vG-ns (see Fig. 1 of Xu and Randall 1998) is quite different from that in cG. The precipitable water in vG-ns decreases gradually in the first five days and then oscillates around  $46.6 \text{ kg m}^{-2}$ . This is about  $8 \text{ kg m}^{-2}$  lower than that in cG. Thus, the lack of solar radiation significantly reduces the SE precipitable water and column temperature. As expected, the simulated temperature (Fig. 5c), moisture (Fig. 5d), and RH (Fig. 7c) are significantly different from those in cG and observations. The reduction of RH occurs mainly in the lower and middle troposphere. The explanation is simple. Without solar radiation, the total (advective plus radiative) cooling is larger, which makes the column more unstable and increases the intensity of cumulus convection. The increase of precipitation cannot be compensated by surface evaporation; thus, less precipitable water remains in the column. On the other hand, if the total cooling were smaller than it should be, as in G97, the SE state would be more humid and warmer.

A comparison of column budgets between cG and vG-ns indicates that the absence of solar radiation and smaller advective effects (about half) greatly alter the individual budget terms. In particular, the surface heat fluxes are greatly enhanced ( $20 \text{ W m}^{-2}$  in  $H_s$  and  $44 \text{ W m}^{-2}$  in  $LE$ ) due to the cooler and drier boundary layer in vG-ns (see Figs. 5c,d).

#### e. Summary of the sensitivity simulations

The results for the SE states of the control and sensitivity simulations can be described by a quasi-linear relationship between precipitable water and column temperature, with all scatter points located between the two extremes provided by S94 and G96 (Fig. 10a). Note that observations from Tropical Oceans Global Atmosphere Coupled Ocean–Atmosphere Response Experiment (TOGA COARE), GATE, and Marshall Islands regions lie in the middle of the scatter. Similar results are also obtained by W.-K. Tao et al. (1999, personal communication) and Tompkins and Craig (1999). Such a quasi-linear relationship between precipitable water and column temperature seems to suggest a constant mass-weighted RH for any SE state. Indeed, the mass-weighted RHs vary slightly (between 66% for vG-ns and 76% for cW) for all simulations. The mass-weighted RH for G97 is 81% while that for S94 is only 60%. The intermodel differences are much greater than those associated with the sensitivity simulations performed in this study.

On the other hand, such differences are not great in terms of the cloud work function quasi equilibrium (Fig. 10b), which can be represented by a negative correlation between the surface RH and the lower-tropospheric lapse rate for a fixed SST [see Arakawa and Chen (1987) for details]. The lapse rate difference of  $0.5 \text{ K km}^{-1}$  among the SE states is not negligible in the Tropics. Thus, a concise description of the results shown in Fig. 10 is that wet columns are thermally stabler, and dry columns are thermally more unstable in the lower troposphere. In the upper troposphere (not shown), however, wet (dry) columns are thermally more unstable (stable).

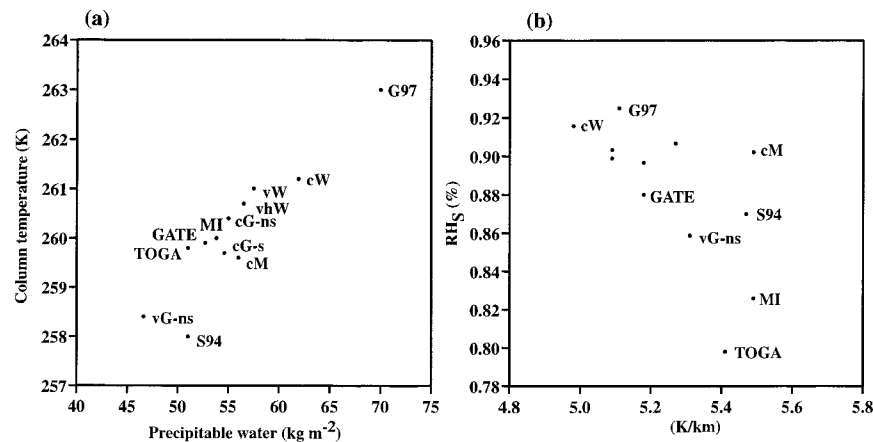


FIG. 10. Scatter diagram of column temperature vs the precipitable water for SE states of all simulations performed in this study, S94 and G96, as well as observations from TOGA COARE, GATE, and Marshall Islands (MI) regions.

## 5. Conclusions and discussion

Statistical-equilibrium (SE) states of radiative–convective systems in tropical oceanic conditions have been simulated with the UCLA–CSU cloud ensemble model (CEM). Typical large-scale conditions from the Marshall Islands and the eastern tropical Atlantic regions are used to drive the UCLA–CSU CEM. The main conclusions of this study are as follows.

- 1) The UCLA–CSU CEM performs reasonably well against observations of two particular tropical oceanic regions in simulating the SE states, driven by the “observed” profiles of the total large-scale advective tendencies over the same regions.
- 2) By imposing a steady large-scale ascent profile, the simulated SE state from this study is somewhere between the cold/dry regime by Sui et al. (1994, S94) and the warm/humid regime by Grabowski et al. (1996, G96).
- 3) The SE states are more sensitive to the transient large-scale forcings than to the magnitudes of the forcing.
- 4) Despite the differences of the SE states among the simulations, the results show that wet columns are thermally more stable (unstable), and dry columns are thermally more unstable (stable) in the lower (upper) troposphere.

In all simulations performed in this study, the SE states are achieved despite some high-frequency fluctuations. The fluctuations are related to the existence of mesoscale convective systems and the diurnal cycle of solar radiation, in addition to the limited domain size used in this study. In the control simulations, the simulated SE precipitable water, column temperature, and relative humidity are only slightly higher than those of the observed mean states in the Marshall Islands and the eastern Atlantic regions. In these simulations, the total (horizontal and vertical) large-scale advective cool-

ing and moistening effects are imposed and assumed to be time invariant. The idealized temporal variation may contribute to some differences between simulations and observations.

Three sensitivity simulations have been performed to compare with similar studies (S94; G96). In these simulations, only the large-scale vertical velocity is imposed, based on the observations from the Marshall Islands region, intended to simulate the SE states over the ascent branch of the Hadley circulations. That is, the horizontal advective effects are totally ignored. It is found that the simulated SE precipitable water, column temperature, and relative humidity are much higher than the observed mean state of the Marshall Islands region, when the large-scale ascent is assumed to be time invariant. This SE state is somewhere between the cold/dry regime by S94 and the warm/humid regime by G96. In addition, the profiles of relative humidity and the mixing ratios of the various water species are very different among the three studies, especially in the upper troposphere.

With a specified temporal variation of the large-scale vertical velocity that allows for subsidence, the simulated SE state becomes colder and drier because moisture and condensate are not accumulated during extended suppressed periods. This simulation captures some temporal variabilities associated with the easterly waves in the Marshall Islands region. Another simulation was performed with reduced large-scale vertical motion while assuming the same temporal variation. The simulated SE state remains about the same. More realistic temporal variabilities of the large-scale forcings and the wind profiles do not significantly change the mean relative humidity profile over the eastern Atlantic region, compared with the two idealized simulations with time-invariant large-scale forcings and specified wind profiles.

In general, all simulated SE states under any type of

large-scale conditions (forcings and wind profiles) exhibit that wet columns are thermally more stable (unstable) and dry columns are thermally more unstable (stable) in the lower (upper) troposphere. The quasi-linear relationship between precipitable water and column temperature implies a constant mass-weighted RH, especially for convectively disturbed regions. This result may have serious implications for tropical dynamics, especially regarding the short-term and long-term variabilities of the tropical atmosphere. For short time-scales, precipitable water and column temperature tend to be negatively correlated (Xu and Randall 1998), based upon observations and CEM simulations, because the short-scale variations are mainly related to cumulus convection. On the other hand, the SE states of convective regions of the Tropics are less dependent upon the large-scale conditions (and thus the intensity of cumulus convection) since they are determined by the long-term balance between radiation, surface flux, and cumulus convection.

In addition, the presence of the vertical shear of the horizontal wind does not significantly change the simulated SE states, provided that the surface wind speeds are identical. This preliminary conclusion needs to be further investigated because only two sheared profiles have been examined in this study.

Column mean budgets suggest that the feedback of simulated temperature and moisture on the vertical advective effects is rather strong. This point is based upon an intermodel comparison of three similar simulations with an identical large-scale vertical ascent profile. Any model deficiencies and/or differences in design of simulations (e.g., the imposed geostrophic wind profile) can strongly influence the simulated SE states.

The cold and dry regime simulated by S94 is related to the inability of its model to maintain the initial wind profile, which greatly reduces the surface wind speed (Tao et al. 1999). This does not reduce the surface heat fluxes much because the simulated boundary layer is much drier and colder. On the other hand, larger vertical advective effects, due to the dry/cold SE state, increase the convective intensity. The weaker surface wind cannot increase the surface evaporation enough to compensate for the enhanced precipitation so that less precipitable water remains in the column. This explanation is slightly different from that offered by Tao et al. (1999).

Finally, numerical simulations for such long-term integrations should be more carefully designed. By imposing a steady large-scale ascent profile, simulated convection is continuously present in the domain so that moisture and hydrometeors (especially ice) are not depleted as much as in the real atmosphere, due to the periodic lateral boundary condition. The accumulation of condensate and its interaction with radiation can significantly alter the SE state. This accumulation did not happen in S94 because the simulated ice content was extremely small. Thus, an ideal design of numerical

simulations is to allow time-varying large-scale vertical motion and horizontal advective effects such that the feedback of simulated temperature and moisture on the vertical advective effects is present and condensate is not accumulated. Sensitivity simulations with different external forcings such as higher/lower SSTs (e.g., Lau et al. 1994) will be more meaningful than those with a steady large-scale ascent alone. Such a study is underway with the UCLA-CSU CEM. Results will be reported in a separate paper.

*Acknowledgments.* The authors would like to thank Drs. C.-H. Sui, W.-K. Tao, S. Krueger, and W. Grabowski for helpful discussions during the course of the research, and Dr. C.-H. Sui for kindly providing the Marshall Islands data used in the study.

This research was supported by the Environmental Sciences Division of the U.S. Department of Energy under Grant DE-FG03-95ER61968 as part of the Atmospheric Radiation Measurement Program. The computations were performed at the National Energy Research Supercomputer Center, Berkeley, CA.

#### REFERENCES

- Arakawa, A., and J.-M. Chen, 1987: Closure assumptions in the cumulus parameterization problem. *Short- and Medium-Range Numerical Prediction, WMO/IUGG Numerical Weather Prediction Symp.*, Tokyo, Japan, WMO, 107–131.
- Esbensen, S. K., and K. Ooyama, 1983: An objective analysis of temperature and relative humidity data over the B and A/B ship arrays during Phase III of GATE. Department of Atmospheric Sciences, Oregon State University, Corvallis, Oregon, 87 pp. [Available from College of Oceanic and Atmospheric Sciences, Oregon State University, Corvallis, OR 97331.]
- Grabowski, W., M. W. Moncrieff, and J. T. Kiehl, 1996: Long-term behavior of precipitating tropical cloud systems: A numerical study. *Quart. J. Roy. Meteor. Soc.*, **122**, 1019–1041.
- Harshvardhan, R. Davies, D. A. Randall, and T. G. Corsetti, 1987: A fast radiation parameterization for general circulation models. *J. Geophys. Res.*, **92**, 1009–1016.
- Held, I. M., R. S. Hemler, and V. Ramaswamy, 1993: Radiative-convective equilibrium with explicit two-dimensional moist convection. *J. Atmos. Sci.*, **50**, 3909–3927.
- Islam, S., R. L. Bras, and K. A. Emanuel, 1993: Predictability of mesoscale rainfall in the Tropics. *J. Appl. Meteor.*, **32**, 297–310.
- Krishnamurti, T. N., V. Wong, H. L. Pan, G. van Dam, and D. McClellan, 1976: Sea surface temperatures for GATE. Report 76-3, Department of Meteorology, The Florida State University, 268 pp. [Available from Department of Meteorology, The Florida State University, Tallahassee, FL 32306.]
- Krueger, S. K., 1988: Numerical simulation of tropical cumulus clouds and their interaction with the subcloud layer. *J. Atmos. Sci.*, **45**, 2221–2250.
- , Q. Fu, K. N. Liou, and H.-N. Chin, 1995: Improvements of an ice-phase microphysics parameterization for use in numerical simulations of tropical convection. *J. Appl. Meteor.*, **34**, 281–287.
- Lau, K.-M., C.-H. Sui, M.-D. Chou, and W.-K. Tao, 1994: An inquiry into the cirrus-cloud thermostat effect for tropical sea surface temperature. *J. Geophys. Lett.*, **21**, 1157–1160.
- Lin, Y.-L., R. D. Farley, and H. D. Orville, 1983: Bulk parameterization of the snow field in a cloud model. *J. Climate Appl. Meteor.*, **22**, 1065–1092.
- Manabe, S., and R. F. Strickler, 1964: Thermal equilibrium of the

- atmosphere with a convective adjustment. *J. Atmos. Sci.*, **21**, 361–385.
- , and R. T. Wetherald, 1967: Thermal equilibrium of the atmosphere with a given distribution of relative humidity. *J. Atmos. Sci.*, **24**, 241–259.
- Nakajima, K., and T. Matsuno, 1988: Numerical experiments concerning the origin of cloud clusters in the tropical atmosphere. *J. Meteor. Soc. Japan*, **66**, 309–329.
- Ramanathan, V., and J. A. Oakley Jr., 1978: Climate modeling through radiative convective models. *Rev. Geophys. Space Phys.*, **16**, 465–489.
- Randall, D. A., Q. Hu, K.-M. Xu, and S. K. Krueger, 1994: Radiative-convective disequilibrium. *Atmos. Res.*, **31**, 315–327.
- Rennó, N. O., K. A. Emanuel, and P. H. Stone, 1994: A radiative-convective model with an explicit hydrological cycle, 1. Formulation and sensitivity to model parameters. *J. Geophys. Res.*, **99**, 14 429–14 441.
- Robe, F. R., and K. A. Emanuel, 1996: Dependence of tropical convection on radiative forcing. *J. Atmos. Sci.*, **53**, 3265–3275.
- Somerville, R., and L. Remer, 1984: Cloud optical thickness feedbacks in the CO<sub>2</sub> climate problem. *J. Geophys. Res.*, **89**, 9669–9672.
- Sui, C.-H., K.-M. Lau, W.-K. Tao, and J. Simpson, 1994: The tropical water and energy cycle in a cumulus ensemble model. Part I: Equilibrium climate. *J. Atmos. Sci.*, **51**, 711–728.
- Thompson, R. M., Jr., S. W. Payne, E. E. Recker, and R. J. Reed, 1979: Structure and properties of synoptic-scale wave disturbances in the intratropical convergence zone of the eastern Atlantic. *J. Atmos. Sci.*, **36**, 53–72.
- Tompkins, A. M., and G. C. Craig, 1998: Radiative-convective equilibrium in a three-dimensional cloud-ensemble model. *Quart. J. Roy. Meteor. Soc.*, **124**, 2073–2097.
- , and —, 1999: Sensitivity of tropical convection to sea surface temperature in the absence of large-scale flow. *J. Climate*, **12**, 462–476.
- Xu, K.-M., 1995: Partitioning mass, heat, and moisture budgets of explicitly simulated cumulus ensembles into convective and stratiform components. *J. Atmos. Sci.*, **52**, 551–573.
- , and S. K. Krueger, 1991: Evaluation of cloudiness parameterizations using a cumulus ensemble model. *Mon. Wea. Rev.*, **119**, 342–367.
- , and D. A. Randall, 1995a: Impact of interactive radiative transfer on the macroscopic behavior of cumulus ensembles. Part I: Radiation parameterization and sensitivity tests. *J. Atmos. Sci.*, **52**, 785–799.
- , and —, 1995b: Impact of interactive radiative transfer on the macroscopic behavior of cumulus ensembles. Part II: Mechanisms for cloud–radiation interactions. *J. Atmos. Sci.*, **52**, 800–817.
- , and —, 1996: Explicit simulation of cumulus ensembles with the GATE Phase III data: Comparison with observations. *J. Atmos. Sci.*, **53**, 3710–3736.
- , and —, 1998: Influence of large-scale advective cooling and moistening effects on the quasi-equilibrium behavior of explicitly simulated cumulus ensembles. *J. Atmos. Sci.*, **55**, 896–909.
- , A. Arakawa, and S. K. Krueger 1992: The macroscopic behavior of cumulus ensembles simulated by a cumulus ensemble model. *J. Atmos. Sci.*, **49**, 2402–2420.
- Yanai, M., S. Esbensen, and J.-H. Chu, 1973: Determination of bulk properties of tropical cloud clusters from large-scale heat and moisture budgets. *J. Atmos. Sci.*, **30**, 611–627.
- , J.-H. Chu, T. E. Stark, and T. Nitta, 1976: Response of deep and shallow tropical maritime cumuli to large-scale processes. *J. Atmos. Sci.*, **33**, 976–991.